

RESEARCH ARTICLE

The Effect of Landing Gear Dimension Variation on the Static Strength and Dynamic Response of Unmanned Aerial Vehicle (UAV)

L. Son*, M. Rusli, S.P. Putra and E. Satria

Mechanical Engineering Department, Engineering Faculty, Universitas Andalas, 25163, Padang, Indonesia

ABSTRACT - This research discusses the static and dynamic analysis of the landing gear structure of an unmanned aerial vehicle (UAV). The dimensional study is conducted to investigate the effect of landing gear dimension variation on UAVs' static strength and dynamic response. Static analysis was performed with Finite Element Method (FEM) software. The dynamic response of the UAV is analyzed using a single-degree-of-freedom vibration model. Based on the static analysis results, the landing gear stiffness and strength can be increased by increasing the width and decreasing the height, radius, and length of the landing gear structure. The energy dissipation in the dynamic analysis is described by hysteresis and viscous damping model. The dynamic response simulation results show that the increase in the stiffness of the landing gear leads to an increase in force transmission and acceleration of the UAV. Furthermore, the UAV response using the viscous damping model can accurately predict the system's response with the hysteretic damping model for small damping conditions. However, the deviation was observed for large damping conditions.

ARTICLE HISTORY

Received : 22nd Nov 2022
 Revised : 08th Sept 2023
 Accepted : 26th Sept 2023
 Published : 18th Oct 2023

KEYWORDS

UAV;
 Landing gear;
 Response;
 Static;
 Dynamic

1.0 INTRODUCTION

An Unmanned Aerial Vehicle (UAV) is an autonomous airplane controlled from a control station using a remote control or computer. UAVs have many variants of form, size, configuration, and characteristics, which depend on their application. One of the most critical components of a UAV is the landing gear. Two main functions of the landing gear are to support the weight and absorb the impact energy during landing [1,2]. Apart from reducing vibrations due to landing, the landing gear must also be light enough so that it does not have a significant effect on increasing the weight of the aircraft [3].

Several studies on landing gear have been carried out by many researchers throughout the world because of its very crucial function in aircraft operations. Stress analysis of light unmanned aerial vehicles during landing was investigated by Sonowal et al. [4]. Lee et al. [5] researched crack growth in landing gear components. Baskaran et al. [6] investigated the frictional resistance gained by the landing gear struts while an aircraft is landing at various sink rates. Analysis of the landing gear strength criteria by performing the structural analysis reported by Aydin et al. [7]. Crashworthiness analysis of UCAV's main landing gear using explicit dynamics conducted by Swati et al. [8]. Chen and Xue [9] performed dynamic simulation and optimization of landing gear using a BP neural network and genetic algorithm. Yu et al. [10] have shown that the application of a shock absorber with an inward-folding composite tube in a legged landing gear system can reduce the initial peak load and increase energy absorption. Jiang et al. [11] establish a multibody dynamic model (MBD) and evaluate the effect of landing gear torsional damping on the aircraft's directional stability.

The impact force generated during landing causes a significant acceleration on the UAV's body. This effect leads to broken the UAV body and landing gear structures. Furthermore, the impact-induced vibration on the UAV body causes damage to the electrical components inside the UAV and reduces the UAV steering stability after landing. Several methods are available to minimize the damage caused by the impact force on the aircraft body and landing gear structure during landing. Luong et al. [12] developed a robust adaptive control for an aircraft landing gear with a magnetorheological damper. Mikulowski and Jankowski [13] investigate some adaptive control strategies for reducing impact-induced vibration in landing gear systems. Yazici and Sever [14] developed an active control of a non-linear landing gear system having an oleo-pneumatic shock absorber. Son et al. [15] propose a new concept for UAV landing gear shock vibration control using a pre-straining spring momentum exchange impact damper.

Strengthening the landing gear structure can reduce the deformation of the landing gear during the landing stage [16]. However, increasing the landing gear structural stiffness leads to a rise in the force transmission and acceleration of the UAV body. This effect can cause damage to the electrical components inside the UAV [17]. This research is conducted to investigate the influence of U-shaped landing gear dimension variation on the static strength and dynamic response of UAVs. A U-shaped structure for a UAV landing gear system is intended to produce sufficient rigidity with light weight suitable for use on a small unmanned aerial vehicle. The position of U-shaped landing gear on the UAV fuselage is shown in Figure 1(a). The landing gear dimensions are shown in Figure 1(b).

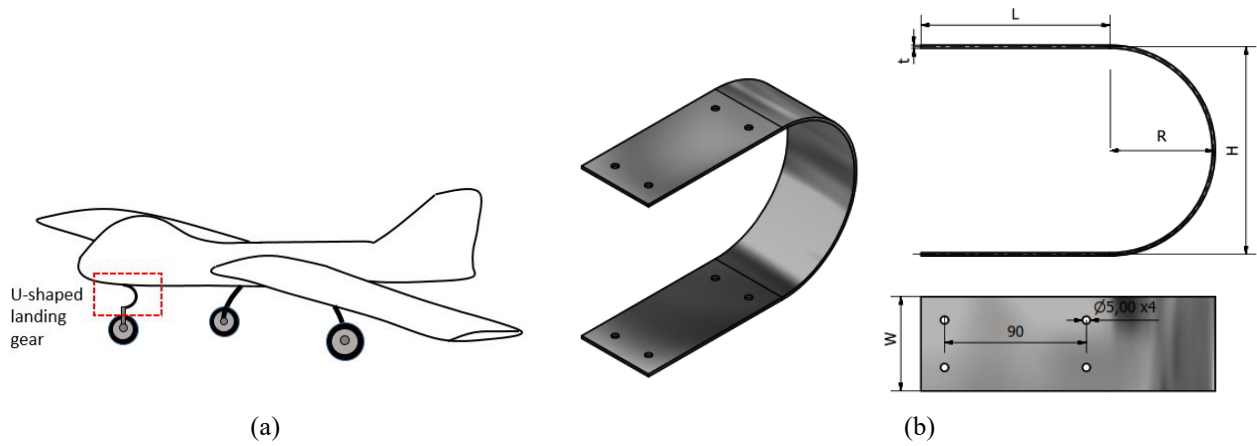


Figure 1. U-shape landing gear

2.0 ANALYSIS OF THE LANDING PROCESS

The landing gear is one of several UAV components that play an essential role during UAV manoeuvrings, such as taxiing, take-off, and landing. During its operation, the landing gear receives two types of load, i.e., static and dynamic. The static load of the landing gear comes from the plane weight, and the dynamic load is induced by the impact force generated during landing, as shown in Figure 2 [15].

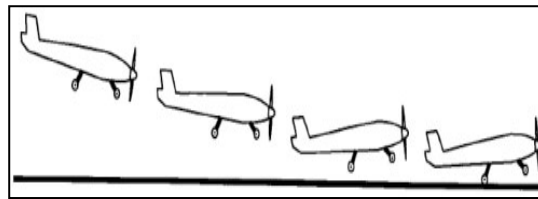


Figure 2. Landing process of UAV

2.1 Static Analysis of Landing Gear Structure

The static analysis of the landing gear structure is conducted by utilizing the force and displacement curve (*F-s*) as depicted in Figure 3. As shown in Figure 3, elastic deformation occurs for small deformation. In this elastic region, the material’s stiffness is linear, and the material can recover to its original form after the load is released. The yield point is the limit point between the elastic and inelastic regions. When the applied load passes its yield point, the material becomes plastic, and it cannot change back to its original form after the applied load is released.

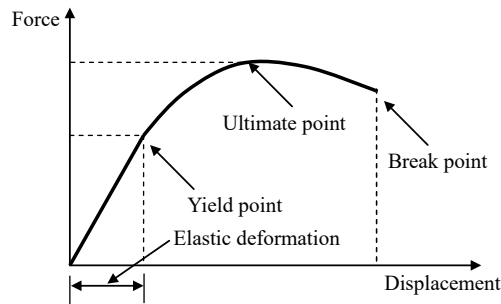


Figure 3. Force-displacement curve [18]

The equivalent stiffness of the U-shape landing gear at the elastic region can be calculated theoretically by considering the relation between the shear force and bending moment with the translational and rotational displacement acting on the landing gear element, as shown in Figure 4. In this theoretical study, it is assumed that the external and internal forces are in equilibrium. Besides that, the supports must be rigid, and no movement is possible. Another assumption is the materials are strained well within the elastic region. As depicted in Figure 4, the force stiffness (k_1) and moment stiffness (k_3) due to the unit vertical displacement are calculated using the unit-load or virtual works method. According to this method, the vertical displacement of the landing gear structure is expressed by [19]:

$$v = \int \frac{M(x) \overline{M}_1(x)}{EI} dx$$

$$v = 2 \int_0^{l_0} \frac{(-k_1 x + k_3)(-x)}{EI} dx + \int_0^\pi \frac{[-k_1(l_0 + r \sin \theta) + k_3][-(l_0 + r \sin \theta)]}{EI} r d\theta$$

$$v = \left(\frac{2l_0^3}{3EI} + \frac{r\pi l_0^2 + 4r^2 l_0}{EI} + \frac{r^3 \pi}{2EI} \right) k_1 - \frac{l_0^2 + r\pi l_0 + 2r^2}{EI} k_3 = 1 \tag{1}$$

$M(x)$ and $M_1(x)$ in Eq. (1) are the applied and virtual bending moments. The rotational displacement is calculated by [19].

$$\theta = \int \frac{M(x) \overline{M_2(x)}}{EI} dx$$

$$\theta = 2 \int_0^{l_0} \frac{(-k_1 x + k_3)(1)}{EI} dx + \int_0^\pi \frac{[-k_1(l_0 + r \sin \theta) + k_3(1)]}{EI} r d\theta$$

$$\theta = - \left(\frac{l_0^2 + l_0 r \pi + 2r^2}{EI} \right) k_1 + \frac{2l_0 + r\pi}{EI} k_3 = 0 \tag{2}$$

k_1 and k_3 are obtained by solving Eq. (1) and (2), hence

$$k_1 = \frac{6EI(2l_0 + r\pi)}{2l_0^4 + 4r\pi l_0^3 + 24r^2 l_0^2 + 6r^3 \pi l_0 + 3r^4 \pi^2 - 24r^4} \tag{3}$$

$$k_3 = \frac{6EI(l_0^2 + r\pi l_0 + 2r^2)}{2l_0^4 + 4r\pi l_0^3 + 24r^2 l_0^2 + 6r^3 \pi l_0 + 3r^4 \pi^2 - 24r^4} \tag{4}$$

The stiffness k_2 and k_4 are calculated using the same method as the previous procedure, therefore

$$k_2 = \frac{6EI(l_0^2 + r\pi l_0 + 2r^2)}{2l_0^4 + 4r\pi l_0^3 + 24r^2 l_0^2 + 6r^3 \pi l_0 + 3r^4 \pi^2 - 24r^4} \tag{5}$$

$$k_4 = \frac{EI(4l_0^3 + 6r\pi l_0^2 + 24r^2 l_0 + 3r^3 \pi)}{2l_0^4 + 4r\pi l_0^3 + 24r^2 l_0^2 + 6r^3 \pi l_0 + 3r^4 \pi^2 - 24r^4} \tag{6}$$

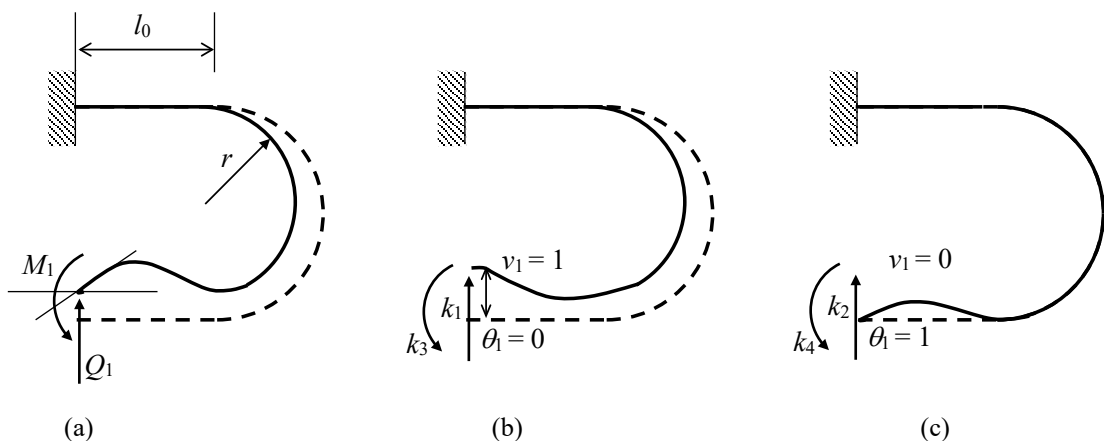


Figure 4. Force and displacement relationship using the unit-load method

For the U-shape landing gear model, as shown in Figure 4, the horizontal force is assumed to be zero; the force-displacement relationship can be expressed as:

$$\begin{Bmatrix} P_u \\ P_v \\ M \end{Bmatrix} = \begin{bmatrix} 0 & 0 & 0 \\ 0 & k_1 & -k_2 \\ 0 & -k_3 & k_4 \end{bmatrix} \begin{Bmatrix} u \\ v \\ \theta \end{Bmatrix} \tag{7}$$

In Eq. (7), P_u , P_v , and M are the horizontal force, vertical force, and bending moment acting on the free end of the landing gear structure. Meanwhile, u , v , and q are the related horizontal, vertical, and rotational displacements, respectively. Eq. (7) can be simplified as follows:

$$P_v = k_1 v - k_2 \theta \tag{8}$$

$$M = -k_3 v + k_4 \theta \tag{9}$$

Because the clamp can be assumed as a rigid plate, the spring displacement (d) can be calculated as:

$$\delta = v \tag{10}$$

and

$$\theta = \frac{\delta}{L} \tag{11}$$

The bending moment induced by the external load acting on the articulated constraint point is

$$M_D = PL = P_v L + M \tag{12}$$

According to Eqs. (7) to (12), the equivalent stiffness of the landing gear structure can be written as:

$$k_{eq} = \frac{P}{\delta} = \frac{k_1 L^2 - k_2 L - k_3 L + k_4}{L^2} \tag{13}$$

Figure 5 shows the force-displacement curve for evaluating the hysteretic energy dissipated by the U-shape landing gear structure during loading (skeleton) and unloading conditions. For the loading condition, the relationship between displacement (u) and force (f_s) is written as [20]:

$$u = \frac{f_s}{k_0} \left(1 + \alpha \left| \frac{f_s}{f_y} \right| \right) \tag{14}$$

where, f_s , f_y , a , and k_0 are the applied force, yield force, non-linear damping factor, and initial stiffness, respectively. For the unloading condition, the displacement vs force relationship is described by the following equation,

$$\frac{u - u^*}{2} = \frac{f_s - f_s^*}{2k_0} \left(1 + \alpha \left| \frac{f_s - f_s^*}{2f_y} \right| \right) \tag{15}$$

The dashed area in Figure 5 is the work (W) that represents the sum of recoverable strain energy (E_s) and the dissipated hysteretic energy (E_H)

$$W = E_s + E_H \tag{16}$$

$$W = \frac{f_s^2}{k_0} \left(\frac{1}{2} + \frac{\alpha}{3} \left| \frac{f_s}{f_y} \right| \right) + \frac{\alpha f_s^2}{3k_0} \left| \frac{f_s}{f_y} \right| \tag{17}$$

$$W = \frac{f_s^2}{k_0} \left(\frac{1}{2} + \frac{2\alpha}{3} \left| \frac{f_s}{f_y} \right| \right) \tag{18}$$

The relationship between recoverable strain energy of the system at (u, f_s) and (u^*, f_s^*) is calculated as:

$$E_s = E_s^* - \frac{1}{2}(u^* - u)(f_s^* + f_s) \tag{19}$$

The energy evaluation during the unloading conditions is conducted by introducing a new coordinate system u', f_s' with the origin at (u^*, f_s^*). The transformation between these two coordinate systems is calculated as

$$u' = u^* - u \tag{20}$$

$$f_s' = f_s^* - f_s \tag{21}$$

By inserting the formula in Eq. (20) and (21) into Eq.(19), the recoverable strain energy during unloading is obtained as

$$E_s - E_s^* = -\frac{1}{2}u'(2f_s^* - f_s') \tag{22}$$

The works and the dissipated energy during unloading conditions are calculated as follows,

$$W' = \frac{(f_s')^2}{k_0} \left(\frac{1}{2} + \frac{\alpha}{3} \left| \frac{f_s'}{f_y} \right| \right) \tag{23}$$

$$E_H' = \frac{\alpha (f_s - f_s^*)^2}{12k_0} \left| \frac{f_s - f_s^*}{f_y} \right| \tag{24}$$

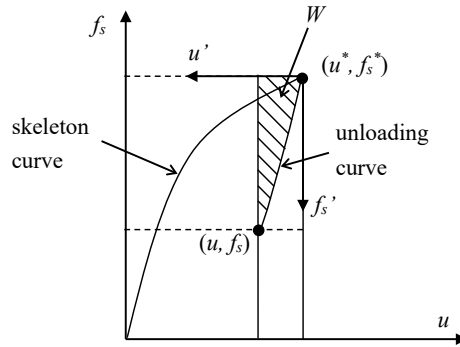


Figure 5. Force and displacement relationship using the unit-load method

For the hysteretic damping model of the landing gear system, as shown in Figure 5, the relationship between the restoring force and the displacement can be derived for two conditions, i.e., loading and unloading conditions. The force-displacement equation in the loading condition is described by,

$$f_s(u) = -\frac{f_y}{2\alpha} \left(1 - \sqrt{1 + \frac{4\alpha k_0}{f_y} u \operatorname{sgn}(u)} \right) \operatorname{sgn}(u) \tag{25}$$

The force-displacement relationship in the unloading region is written as

$$f_s(u) = f_s^* - \frac{f_y}{\alpha} \left(1 - \sqrt{1 + \frac{2\alpha k_0}{f_y} (u - u^*) \operatorname{sgn}(u - u^*)} \right) \operatorname{sgn}(u - u^*) \tag{26}$$

2.2 Dynamic Analysis of Landing Gear Structure

The equation of motion of the UAV system during landing is calculated using the information from Figure 6. As shown in Figure 6, when the landing gear collides with the ground, the dynamic model of the UAV system is affected by the contact force between the landing gear and the floor. However, the contact force becomes zero when the landing gear loses contact with the environment. The governing equations of the system are written as:

$$m\ddot{x} + f_c = 0 \tag{27}$$

Variables m and f_c in Eq. (27) are the UAV mass and contact force, respectively. The contact forces between the landing gear and the ground consist of the elastic and damping forces. In this study, two models of damping force are used to evaluate the contact dynamic that occurred during landing.

i. hysteretic damping model

For the hysteretic damping model, the contact force is calculated using Eq. (25) and (26) as follows:

$$f_c = \begin{cases} f_s(u), & \text{and } u = x \text{ if } x \leq 0 \\ 0, & \text{and } u = 0 \text{ if } x > 0 \end{cases} \tag{28}$$

ii. viscous damping model

For the viscous damping model, the contact condition is modeled using the linear spring (k) and viscous damper (c) elements as follows:

$$f_c = \begin{cases} c\dot{u} + ku, & \text{and } u = x \text{ if } x \leq 0 \\ 0, & \text{and } u = 0 \text{ if } x > 0 \end{cases} \quad (29)$$

The stiffness of the linearized system (k) in Eq. (29) is calculated as the secant stiffness of the non-linear system at the maximum displacement. In this study, the system's deformation is assumed within the elastic range ($u_m = u_y$); the equivalent linear stiffness is calculated using Eq. (30).

$$k = \frac{k_0}{1 + \alpha} \quad (30)$$

The damping coefficient c can be found in Eq. (31) as follows:

$$c = 2\zeta m\omega_n \quad (31)$$

where

$$\zeta = \frac{2\alpha}{3\pi(1 + \alpha)^{3/2}} \frac{T_{av}}{T_0} \quad (32)$$

and

$$\omega_n = \sqrt{\frac{k}{m}} \quad (33)$$

T_{av} and T_0 in Eq. (32) are the average period of excitation frequency and the initial natural period, respectively. The UAV time response is calculated for two conditions. The first condition occurred during the landing gear contact with the ground and experienced free vibration ($x \leq 0$), and the second condition occurred after a collision. For the second condition, the UAV velocity direction is changed after colliding with the ground and experiencing a free-fall motion, ($x > 0$). In this condition, the equation of motion of UAV can be expressed as:

$$x(t) = x_0 + v_0t - \frac{1}{2}gt^2 \quad (34)$$

The system response during contact with the ground is obtained by solving numerically Eq. (27). In the case of the viscous damping model, the system response can be calculated theoretically by

$$x(t) = e^{-\zeta\omega_n t} \{A_1 \cos \omega_d t + A_2 \sin \omega_d t\} - \frac{m \cdot g}{k} \quad (35)$$

A_1 and A_2 in Eq. (35) are the constants that depend on the system's initial conditions.

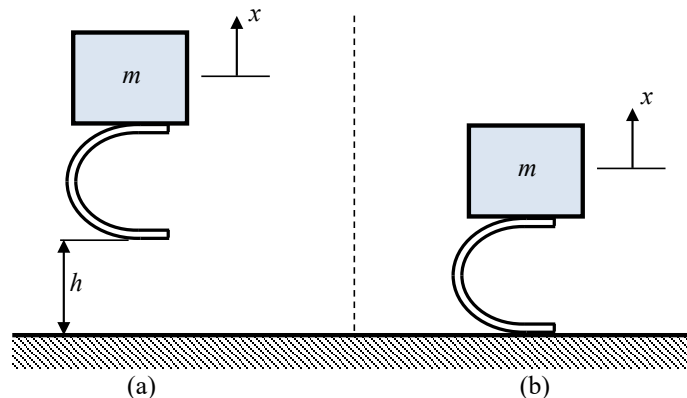


Figure 6. SDOF model of UAV landing process with U-shape landing gear system

3.0 METHODOLOGY

Figure 7 shows the research methodology. The first step is modelling a U-shape landing gear structure. The modeling process is conducted using GiD Pre-Postprocessor software. The second step is the static analysis of the landing gear structure. The static analysis is performed using in-house finite element software. In this step, the landing gear stiffness and maximum elastic force are calculated based on the force and displacement curve obtained from the output of the finite element program [21,22]. The static analysis is conducted by varying the landing gear dimension, such as height (H), radius (R), width (W), and length (L) as shown in Figure. 1. The nominal values of the landing gear dimension are defined as follows: $H = 134$ mm, $R = 65$ mm, $W = 60$ mm, $L = 120$ mm and $t = 2$ mm. The dimensional analysis of landing gear

is conducted using a variation of H , R , W , and L , as shown in Table 1. The selection of landing gear dimensions in Table 1 is carried out by considering the maximum value of the landing gear’s static deflection.

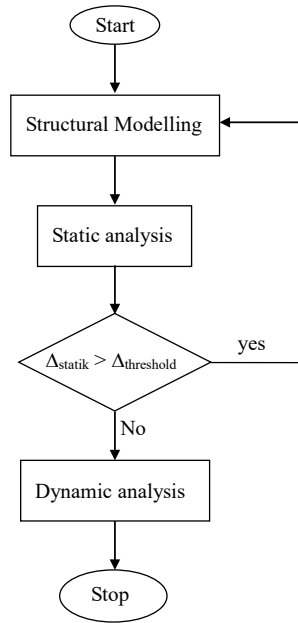


Figure 7. Research methodology

Table 1. Landing gear dimension variation

No.	Model	H (mm)	R (mm)	W (mm)	L (mm)
1	H1R1W1L1	134	65	60	120
2	H2R1W1L1	154	65	60	120
3	H3R1W1L1	174	65	60	120
4	H1R2W1L1	134	55	60	120
5	H1R3W1L1	134	75	60	120
6	H1R1W2L1	134	65	80	120
7	H1R1W3L1	134	65	100	120
8	H1R1W1L2	134	65	60	100
9	H1R1W1L3	134	65	60	140

The safety factor (SF) for each model in Table 1 is calculated to obtain the best dimension configuration for the landing gear. The safety factor is calculated as the ratio between the maximum elastic force and the maximum impulsive force as given by:

$$SF = \frac{P_{max}}{P_{imp}} \tag{36}$$

where

$$P_{imp} = \frac{mv}{\Delta t} \tag{37}$$

v is the vertical velocity of the UAV before contacting with the ground. The impact time Δt is the time length required for the landing gear to come into contact with the ground. The U-shape landing gear is modeled using the 3D finite element method. GiD Pre-Postprocessor software is used for FEM modeling software. The upper surface of the landing gear connected to the fuselage is fixed, and the load is applied vertically to the bottom of the landing gear. Figure. 8 shows the meshing elements of the U-shaped landing gear calculated using GiD Pre-Postprocessor software.

The landing gear dimension configuration described in Table 1 was modeled with the GiD Pre and Post-processor software and calculated using the FEM program. A SODANA FEM program has been developed for this purpose. The maximum elastic force (P_{max}) and spring stiffness (k) are calculated based on the concept of the finite element method involving geometric and material non-linearities. The maximum elastic force and stiffness for each model are determined from the graph obtained from FEM analysis. The theoretical calculation of landing gear stiffness using the unit-load method calculated in Eq. (13) is also conducted for the comparison study. In the last step, the dynamic analysis of the landing gear system is performed with the variation of landing gear dimension and damping. Two damping models were

evaluated in this section, i.e. the hysteretic damping model and the linear viscous damping model, as depicted in Eq. (28) and (29).

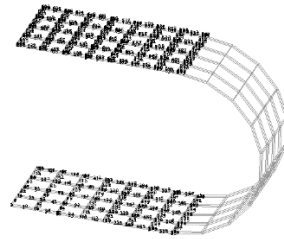


Figure 8. Meshing elements of nose landing gear calculated using GiD Software

4.0 RESULTS AND DISCUSSION

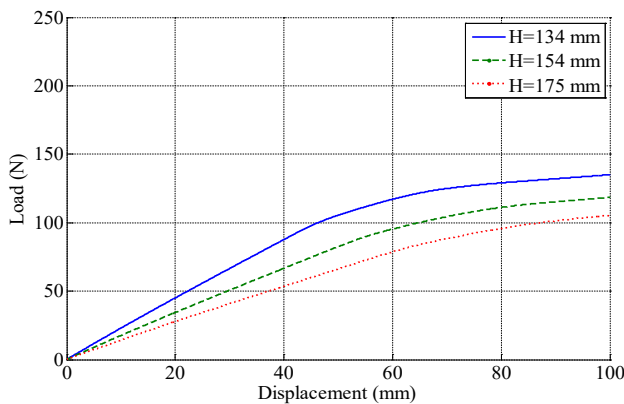
The landing gear’s maximum elastic force and stiffness are numerically calculated using in-house finite element software (SODANA), which has been verified numerically. To investigate the effect of dimension variation on the landing gear stiffness, the numerical simulation is performed for several dimension configurations of the landing gear structure, as shown in Table 1. The numerical study is conducted by applying a quasi-static load to the landing gear structure in the vertical direction. Table 2 shows the mechanical properties of landing gear materials used in the simulation. The relationship between the applied load and the landing gear deformation is shown in Figure 9. The maximum elastic force (P_{max}), the maximum deflection (d_{max}), the stiffness (k), and the safety factor (SF) for several landing gear dimensions in Figure 9 are depicted in Table 3. The safety factor described in Table 3 was calculated using UAV vertical velocity $v = 2$ m/s and the landing gear contact time $\Delta t = 0.15$ s. It is shown from Table 3 that P_{max} and k of model 3(H3R1W1L1) are lower than those obtained using other models.

Table 2. Mechanical properties of landing gear material

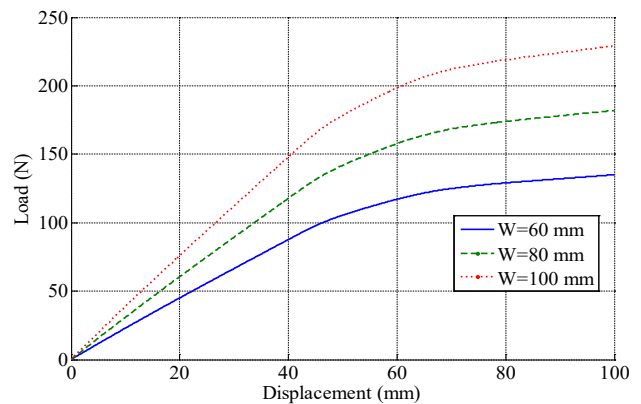
Elastic modulus (MPa)	Poission’s ratio	Yield strength (MPa)
207000	0.3	270

Table 3. Characteristic of landing gear model

No	Model	P_{max} (N)	d_{max} (mm)	k (N/mm)	SF
1	H1R1W1L1	102.2	45.35	2.15	1.92
2	H2R1W1L1	91.9	52.55	1.63	1.72
3	H3R1W1L1	83.1	64.15	1.31	1.56
4	H1R2W1L1	104.8	40.60	2.49	1.97
5	H1R3W1L1	91.7	50.60	1.78	1.72
6	H1R1W2L1	141.8	52.00	2.69	2.66
7	H1R1W3L1	179.9	40.70	3.39	3.37
8	H1R1W1L2	107.0	41.60	2.86	2.01
9	H1R1W1L3	93.5	53.50	1.86	1.75



(a) variation of H



(b) variation of W

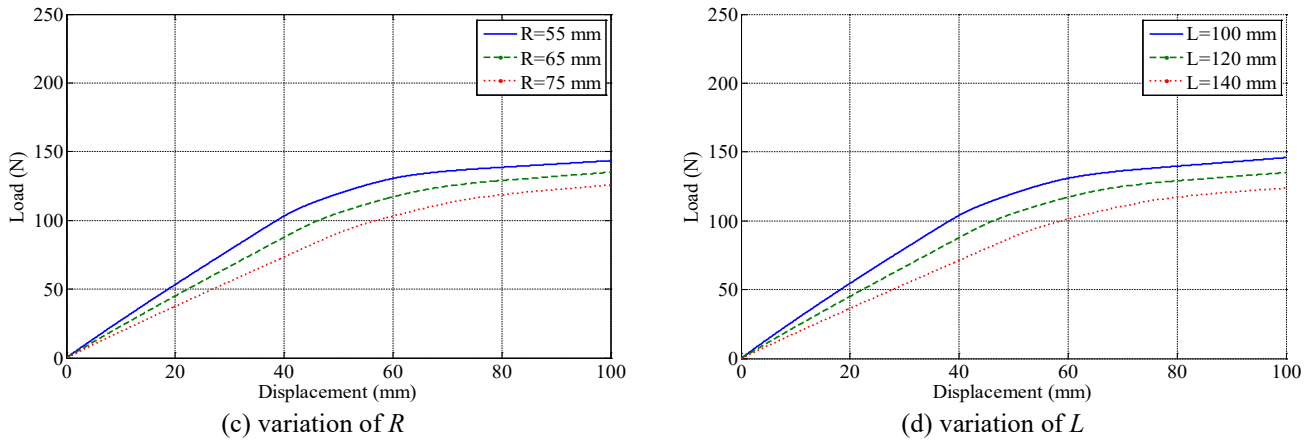


Figure 9. The effect of landing gear dimension on the force-displacement curve

According to the results shown in Table 3, the landing gear strength and stiffness can be increased by increasing the width (W) and decreasing the height (H), radius (R), and length (L) of the landing gear structure. The maximum safety factor is obtained using the landing gear model **H1R1W3L1**. A comparison of the landing gear stiffness calculated by FEM and that from the analytical method is shown in Figure 10(a) and 10(b). The stiffness calculated by the analytical method is lower than that obtained from FEM analysis. These results may be due to several assumptions used in the analytical approach. The error percentage of analytical calculation compared with that calculated by FEM is 35%, as shown in Figure 10. Further inspection from Figure 10 shows that even though the discrepancy between FEM and the analytical method is relatively large; however, the diagram has the same tendency with the variation of the landing gear dimensions.

Figure 10(a) shows the effect of variation of the landing gear width (W) on the stiffness. It can be observed that the stiffness increases with the increase of landing gear width. The effect of landing gear length (L) on the stiffness is shown in Figure 10(b), where the larger stiffness is observed for the small landing gear length (H1R1W1L2), and the smaller landing gear stiffness is obtained using the largest length (H1R1W1L3).

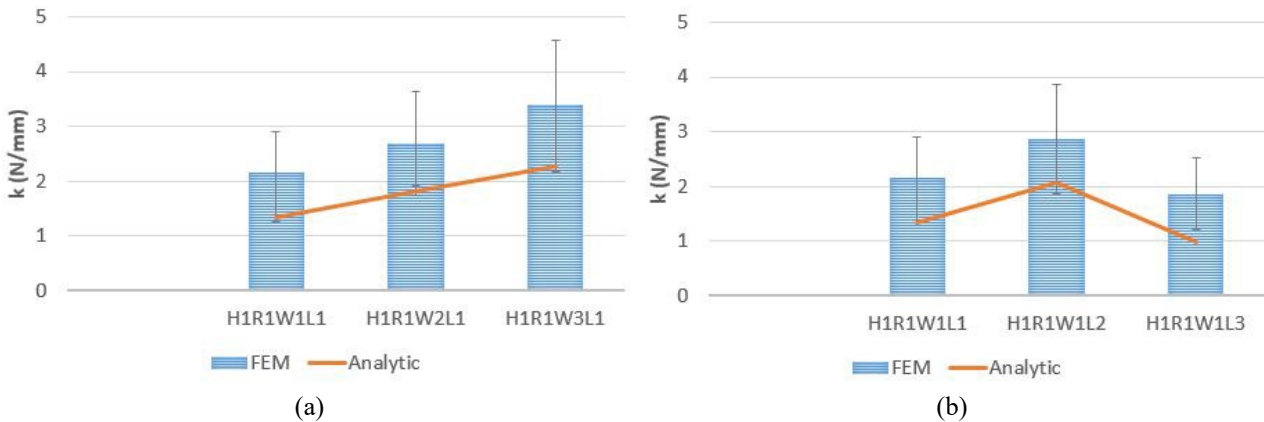


Figure 10. Comparison of landing gear stiffness calculated from FEM and analytical method

Figure 11 shows the force vs displacement curve (hysteretic curve) calculated using $k_0 = 2.34 \text{ kN/mm}$, $f_y = 0.1 \text{ kN}$ and $a = 0.01$ to 1.25. The large area inside the close-loop curve describes the high non-linearity phenomena, which indicates the significant energy dissipation condition. The dynamic response of the UAV is calculated using a one-degree-of-freedom vibration model, as depicted in Figure 6. In the simulation study, the mass parameter (m) is assumed as the portion of UAV mass supported by the landing gear. The stiffness and damping of the landing gear are considered to come from the flexibility and structural damping of the landing gear structure. The wheel stiffness and mass are considered much smaller than the UAV mass, and the values are neglected for the response calculation.

Figure 12 shows the acceleration and displacement response of the UAV system during free fall motion with the variation of non-linear damping factor (a). The system's responses are observed at the main mass. In the simulation study, the UAV mass, the initial stiffness, and the damping factor are $m = 4 \text{ kg}$, $k_0 = 2.34 \text{ kN/m}$ and $a = 0.01$ to 1.25, respectively. The responses are calculated using the initial elevation $h = 0.05 \text{ m}$ which corresponds to the UAV impact velocity $v = 1 \text{ m/s}$. As depicted in Figure 12, for small damping ($a = 0.01$ and $a = 0.05$), the acceleration response curve is smooth, and the UAV mass is reflected after contact with the ground. Meanwhile, for large damping ($a = 0.25$ and $a = 1.25$), the acceleration response curve is distorted due to the high non-linearity of the landing gear system.

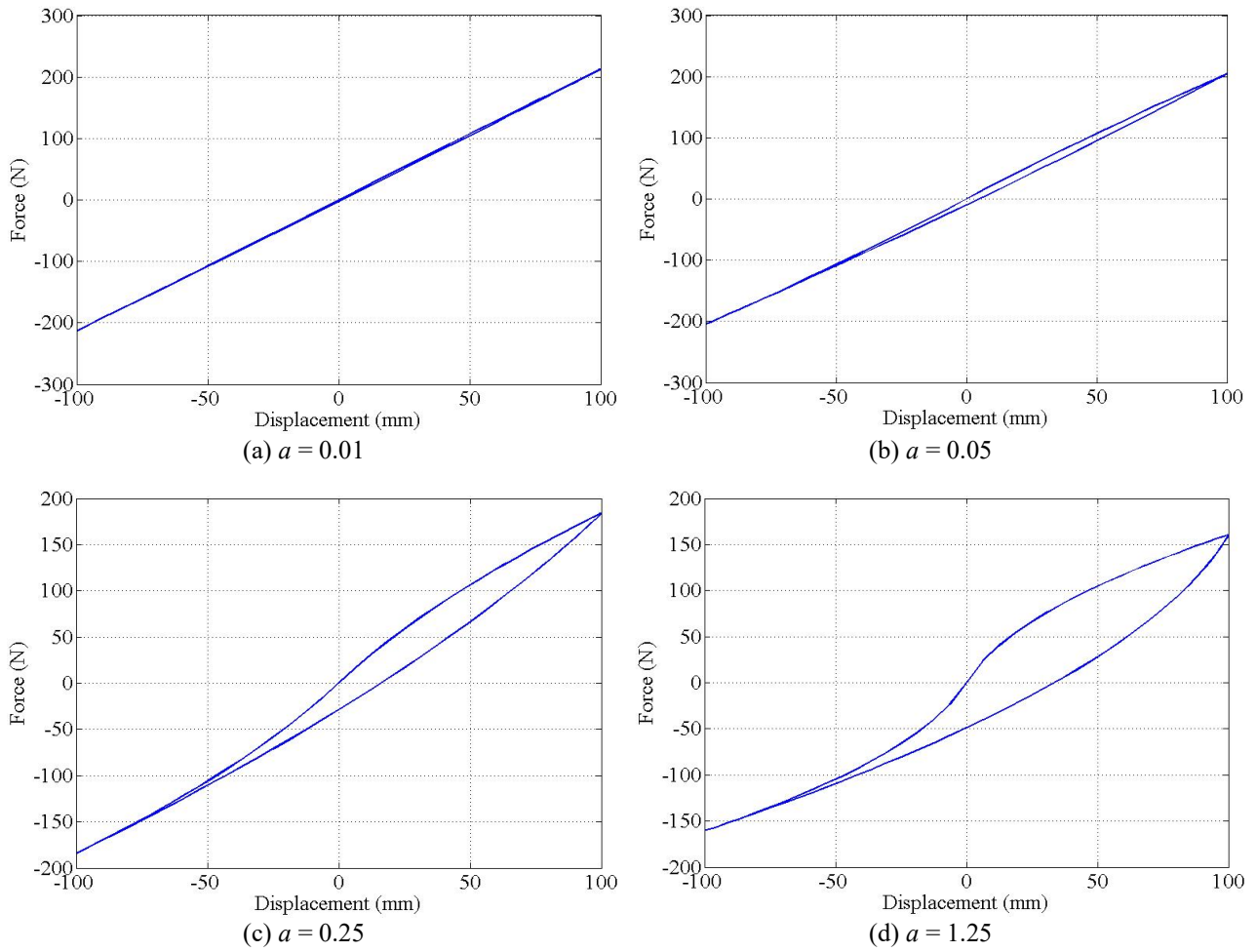


Figure 11. Force vs. displacement curve with the variation of a

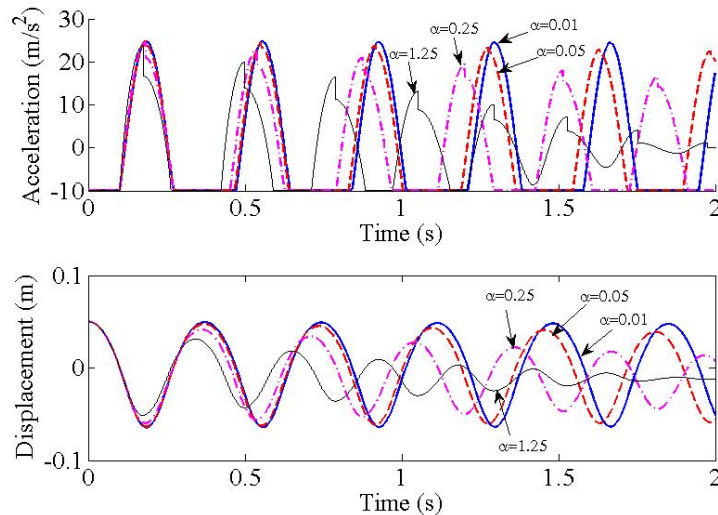


Figure 12. Time response with the variation of a

Figure 13 compares acceleration and displacement responses calculated using non-linear hysteretic damping and linear viscous damping models. The equivalent linear stiffness and damping ratio for the viscous damping model are calculated from Eq. (30) and Eq. (32). The simulation is conducted using a moderate damping factor ($a = 1.25$) to evaluate the effect of the non-linear damping factor on the system response. As seen in Figure 13, the natural frequency of a linear viscous damping model and the non-linear hysteretic damping model are almost the same. Furthermore, as shown in Figure 13(b), similar displacement responses are observed in these two models. However, the acceleration response for the hysteretic damping model, as demonstrated in Figure 13(a), is slightly distorted at the peak curve due to the non-linear effect during the transition from loading and unloading conditions.

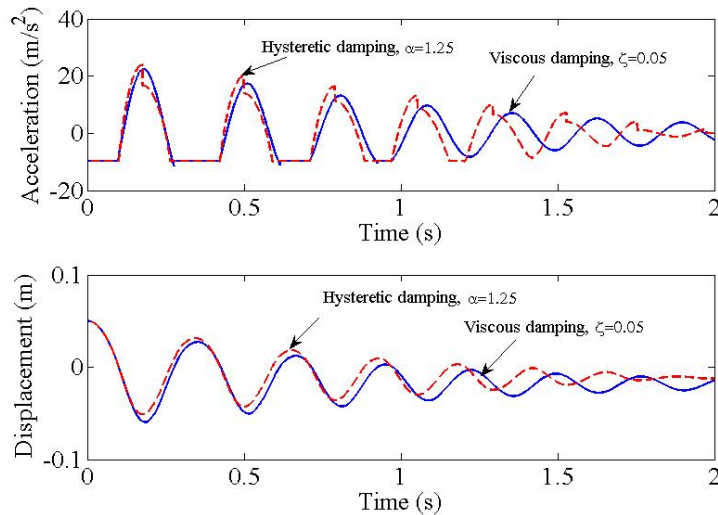
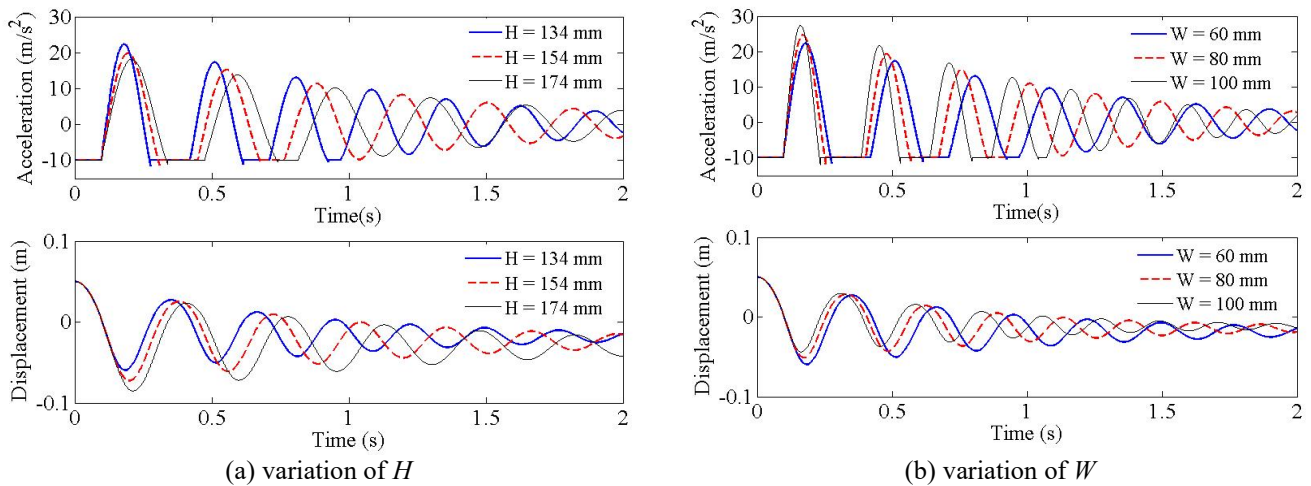


Figure 13. Comparison of response calculated using hysteretic and viscous damping model

Figure 14 shows the acceleration and displacement response of the UAV model for several variations of landing gear dimensions. In this simulation study, the damping component of the landing gear system is modeled using a viscous damping element. The UAV mass, stiffness, and damping ratio used in the simulation are $m = 4 \text{ kg}$, $k_0 = 2.34 \text{ kN/mm}$, and $z = 0.05$. As shown in Figure 14, increasing the landing gear height (H), radius (R), and length (L) and reducing the width (W) will reduce the maximum impact load received by the UAV body.

The effect of the damping ratio on the dynamic response of landing gear is shown in Figure. 15. In this simulation, the damping ratio (z) is varied from 0.025 to 0.2. It is shown in Figure 15 that increasing the damping ratio will reduce the maximum acceleration response. Furthermore, increasing the damping ratio also reduces the steady-state acceleration and displacement responses. However, the most significant acceleration response occurred at the instant after the impact did not change significantly with the variation of damping values. The steering stability of a UAV is influenced by the contact condition between the wheel system and the ground during landing. The steering stability is large if the contact condition between the landing gear and ground ($x \leq 0$) occurs. As can be seen from Figure 15, the steering stability increases using a large damping ratio.



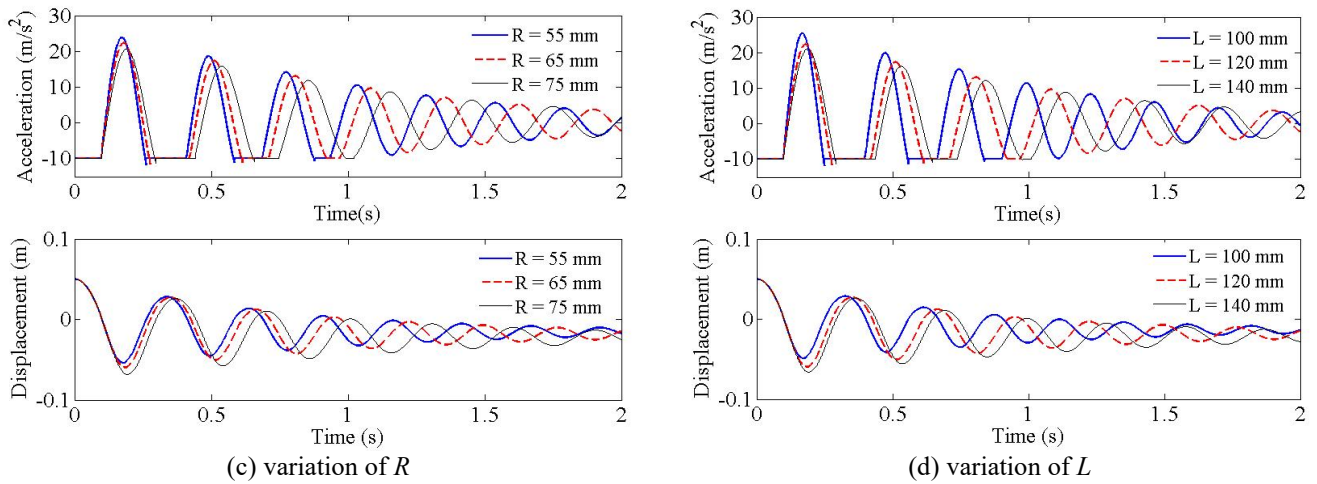


Figure 14. The effect of landing gear dimension on the impact response

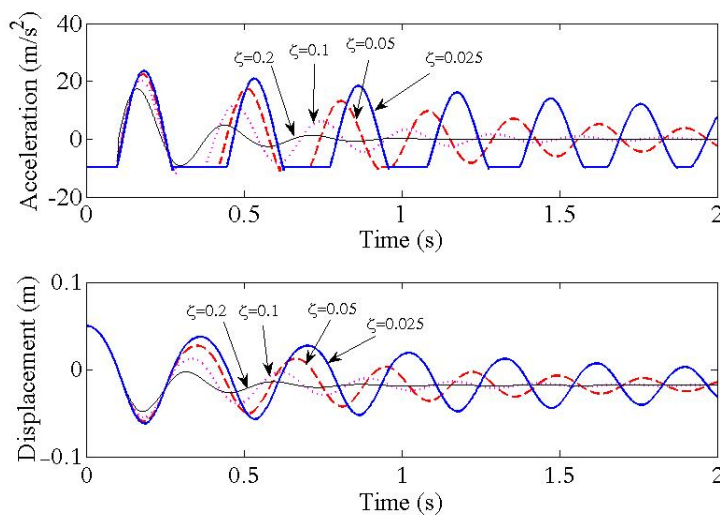


Figure 15. Response system with variation of damping ratio

According to the simulation results, it can be shown that the maximum response amplitude of UAV landing gear using the spring-mass model due to shock loads is largely determined by the stiffness of the spring. Furthermore, the stiffness of the U-shaped landing gear can be varied by changing the spring dimensions. These results are very important in designing the UAV landing gear system because one of the main functions of landing gear is to reduce the shock load during landing.

5.0 CONCLUSIONS

The U-shaped landing gear stiffness can be increased by increasing the width(W) and reducing the height(H), radius(R), and length(L) of the landing gear structure. Increasing the landing gear stiffness causes an increase in the acceleration response and rebound displacement of the UAV. The acceleration and rebound displacement response of UAVs can be reduced by increasing the damping of the landing gear structure. Two damping models are used to evaluate the UAV's response during landing. The displacement responses obtained using viscous damping and hysteretic damping models are almost similar. However, the acceleration responses are slightly different due to the non-linear effect during the transition from loading to unloading conditions.

6.0 ACKNOWLEDGEMENT

Financial support from BOPTN basic research scheme, Andalas University, contract no: 04/UN.16.17/RD/LPPM/2017 is gratefully acknowledged.

7.0 REFERENCES

[1] A. Dubey, B. Badramoni and V. Undavalli, "Landing gear of an aircraft structure: a review," *International Journal of Engineering Research & Technology*, vol. 4, no. 12, pp. 20-25, 2015.

[2] T.H. Hsu, Y.Y. Chang, H.K. Hsu, T.T. Chen and P.W. Hwang, "Predicting the remaining useful life of landing gear with prognostics and health management (PHM)," *Aerospace*, vol. 9, no. 462, pp. 1-16, 2022.

- [3] Y.C. Liang, P.C. Chin, Y.P. Sun and M.R. Wang, "Design and manufacturing of composite landing gear for a light unmanned aerial vehicle," *Applied Sciences*, vol. 11, no. 2, pp. 1-12, 2021.
- [4] P. Sonowal, S. Das, D. K. Mishra and K.M. Pandey, "Stress analysis of landing gear of light unmanned aerial vehicle," *Journal of Physics: Conference Series*. vol. 1455, p. 012019, 2020.
- [5] Y. Lee, J. Park and D. Lee, "Inspection interval optimization of aircraft landing gear component based on risk assessment using equivalent initial flaw size distribution method," *Structural Health Monitoring*, vol. 21, no. 4, pp. 1396-1406, 2021.
- [6] S. Baskaran and S. Sivaprakasam, "Friction analysis of aircraft landing gears due to landing impact," *Proceedings of the Institution of Mechanical Engineers, Part J: Journal of Engineering Tribology*, vol. 236, no. 2, pp. 274-283, 2022.
- [7] G. Aydin and I. Özkol, "Structural analysis of the nose landing gear of a fighter aircraft," *European Journal of Science Technology Special Issue*, vol. 43, pp. 126-135, 2022.
- [8] R.F. Swati, M.A. Amjad, M. Talha, H. Elahi, HR Hamdani, *et al.*, "Crashworthiness study of UCAV's main landing gear using explicit dynamics," *International Journal of Crashworthiness*, vol. 27, no. 6, pp. 1843-1859, 2022.
- [9] J. Chen and C. Xue, "Design optimization and experimental verification of a UAV's landing gear buffer," *International Journal of Crashworthiness*, pp.1-10, 1 Aug 2023.
- [10] Z. Yu, X. Liu, J. Wang, Q. You and Y. Fu, "Shock absorber with inward-folding composite tube and its application in legged landing gear," *International Journal of Crashworthiness*, vol. 26, no. 4, pp. 388-403, 2021.
- [11] Y. Jiang, G. Feng, P. Liu, L. Yuan, J. Ding and B. Jiang, "Influence of nose landing gear torsional damping on the stability of aircraft taxiing direction," *Aerospace*, vol. 9, no. 11, pp. 2-13, 2022.
- [12] Q.V. Luong, D.S. Jang and J. H.Wang, "Robust adaptive control for and aircraft landing gear equipped with a magnetorheological damper," *Applied Sciences*, vol. 10, no. 4, pp. 1-16, 2020.
- [13] G. Mikulowski and L. Jankowski, "Adaptive landing gear: optimum control strategy and potential for improvement," *Shock and Vibration*, vol. 16, pp.175-194, 2009.
- [14] H. Yazici and M. Sever, "Active control of non-linear landing gear system having oleo pneumatic shock absorber using robust linear quadratic regulator approach," *Proceedings of the Institution of Mechanical Engineers, Part G: Journal of Aerospace Engineering*, vol. 232, no. 13, pp.2397-2411, 2018.
- [15] L. Son, M. Bur and M. Rusli, "A new concept for UAV landing gear shock vibration control using pre-straining spring momentum exchange impact damper," *Journal of Vibration and Control*, Vol. 24, no. 8, pp. 1455-1468, 2018.
- [16] A. Pagani, R. Augello, G. Governale and A. Viglietti, "Drop test simulations of composite leaf spring landing gears," *Aerotecnica Missili & Spazio*, vol. 98, pp. 63-74, 2019.
- [17] G. Mikulowski and R. LeLetty, "Advanced landing gears for improved impact absorption," In Proceedings of the 11th International Conference on New Actuators, 2008, pp. 363-366.
- [18] E. Satria, L. Son, M. Bur, and M.D. Akbar, "Finite element analysis to determine stiffness, strength, and energy dissipation of u-shaped steel damper under quasi-static loading," *International Journal of Automotive and Mechanical Engineering*, vol. 18, no. 3, pp. 9042-9050, 2021.
- [19] J. Gao, J. Xi, Y. Xu, J. Ding, J. Zhu, *et al.* "Analysis of the mechanical properties and parameter sensitivity of a u-shaped steel damper," *Frontiers in Materials*, vol. 8, pp. 1-13, 2021.
- [20] F. Segal and D.V. Val, "Modelling earthquake response of structures with hysteretic damping," In Proceedings of 13th World Conference on Earthquake Engineering, no. 4, 2004, Canada.
- [21] S. Kato, Y.B Kim, S. Nakazawa, and T. Ohya, "Simulation of the cyclic behavior of J shaped steel hysteresis devices and study on efficiency for reducing earthquake responses of space structures," *Journal of Constructional Steel Research*, vol 61, no. 10, pp. 1457-1473, 2006.
- [22] E. Satria, L. Son, S. Haris and R. Saputri, "Static and dynamic analysis of steel U-damper for space structures," *International Journal on Advanced Science, Engineering and Technology*, vol. 8, no. 1, pp. 212-218, 2018.